

High-speed two-photon excited autofluorescence imaging of *ex vivo* human retinal pigment epithelial cells toward age-related macular degeneration diagnostic

Olivier La Schiazza

Josef F. Bille

University of Heidelberg
Kirchhoff Institute for Physics
Heidelberg, Germany

Abstract. Age-related macular degeneration (AMD) is among the major concerns in ophthalmology, as it is the primary cause for irreversible blindness in developed countries. Nevertheless, there is poor understanding of the origins and mechanisms that trigger this important ocular disease. In common clinical practice, AMD is monitored by autofluorescence imaging of the retinal pigment epithelial (RPE) cells through a confocal scanning laser ophthalmoscope. The RPE cells derive their dominant autofluorescence from the lipofuscin granules that accumulate in the cytoplasm with increasing age and disease. We explored a different approach to retinal RPE imaging using two-photon excited autofluorescence, offering intrinsic three-dimensional resolution, larger sensing depth and reduced photodamage compared to single-photon excited fluorescence ophthalmoscopy. A two-photon microscope, based on the architecture of a conventional scanning laser ophthalmoscope (HRT, Heidelberg Engineering, Germany), was designed for autofluorescence imaging on retina samples from post-mortem human-donor eyes. We were able to visualize at video-rate speed single RPE lipofuscin granules, demonstrating the potential to develop this method toward clinical practice for patients with RPE-related retinal disease like AMD. © 2008 Society of Photo-Optical Instrumentation Engineers. [DOI: 10.1117/1.2999607]

Keywords: Two-photon excited fluorescence; scanning laser ophthalmoscope; RPE; lipofuscin; age-related macular degeneration.

Paper 07348R received Aug. 23, 2007; revised manuscript received Apr. 16, 2008; accepted for publication Aug. 26, 2008; published online Nov. 5, 2008.

1 Introduction

The retinal pigment epithelium (RPE), located between the neurosensory retina and Bruch's membrane, plays an important role in the metabolic functioning and integrity of the photoreceptors and assures their excitability.¹ It is therefore essential for visual function. In the aging eye, lipofuscin accumulates in the lysosomal compartment of the RPE cells as a byproduct of phagocytosis of shed photoreceptor outer-segment disks.²⁻⁴ It has been assumed that excessive levels of lipofuscin, and more specifically its phototoxic component A2-E, cause dysfunction of the RPE cells and may contribute to the pathogenesis of age-related macular degeneration (AMD).⁵⁻⁹ AMD is characterized by the progressive degeneration of the RPE cells in the macular region, which results in an irrevocable loss of central vision. The first clinical indication for AMD is the accumulation of large drusen (waste material) between the RPE and Bruch's membrane. The relationship between lipofuscin accumulation and drusen formation, however, remains controversial. One hypothesis widely accepted among ophthalmologists suggests that a dysfunction of the RPE is responsible for drusen formation.⁴

AMD is the principle cause for irreversible loss of vision in developed countries. Around 35% of the human population over 75 years of age has some degree of AMD.¹⁰ It is therefore important to develop new powerful *in vivo* early diagnostic and monitoring methods, providing the potential of understanding the origins and mechanisms of this sight-impairing disease on a subcellular level in order to eventually prevent its onset.

Fundus autofluorescence (FAF) imaging is a recent useful diagnostic tool for noninvasively monitoring RPE-related retinal pathologies, and more specifically AMD, by analyzing the FAF patterns from the macula region through a modified fundus camera or a confocal scanning laser ophthalmoscope.¹¹⁻¹⁵ Endogenous chromophores of the lipofuscin granules in the RPE cells demonstrate strong autofluorescence when excited with blue light.¹⁶ FAF imaging gives an indication of the biological and functional properties of the RPE cells, and their modification is an indication of aging and disease, providing insight into pathogenic mechanisms of RPE dysfunction.^{17,18}

Below we demonstrate a novel technique for noninvasive functional imaging of RPE cells using two-photon excited fluorescence (TPEF). The two-photon excitation process consists of the simultaneous absorption of two lower-energy

Address all correspondence to: Olivier La Schiazza, University of Heidelberg, Kirchhoff Institute for Physics, Heidelberg, Germany; Tel: +49 6221 549273; Fax: +49 6221 549112; E-mail: olivier.la.schiazza@kip.uni-heidelberg.de.

(longer wavelength) photons whose combined energy is sufficient to induce a molecular transition to an excited state that would otherwise require a single photon of lower wavelength. This process was first theoretically predicted by Göppert-Mayer in 1931,¹⁹ and 30 years later, with the availability of lasers allowing high light intensities, it was experimentally verified by Kaiser and Garrett.²⁰ In 1990 Denk et al. were the first to apply this technology to scanning laser microscopy.²¹ From there on, TPEF, and more generally multiphoton microscopy, experienced a tremendous success in biological research, to become the technique of choice in fluorescence microscopy for thick tissues and live animals.²² Its huge impact is mainly derived from its unique characteristic of localized excitation. As the fluorescence emission is quadratically dependent on the illumination intensity, two-photon absorption is only confined to the vicinity of the focal plane,²¹ in contrast to single-photon absorption which occurs through the entire excitation light cone. This feature is at the basis of a number of major advantages for bioimaging applications, as it results in an intrinsic three-dimensional diffraction-limited resolution, providing optical sectioning of thick tissues without the need for a confocal pinhole to spatially filter the emission light because no out-of-focus background fluorescence is produced. Furthermore, the use of near-infrared (NIR) excitation light, instead of UV or visible light typically employed in single-photon fluorescence microscopy, not only reduces cell damage but also promotes a larger sensing depth in thick biological samples due to less scattering and the lack of efficient endogenous absorbers in this spectral range.^{23,24} Photobleaching and photodamage may only occur in the focal plane where photointeraction takes place. Exceptions, however, are pigmented cells containing melanin, where linear NIR absorption is likely to occur.

Regarding these unique characteristics of TPEF and the transparency of the human eye to NIR light, two-photon retinal imaging has undiscovered potential for noninvasive high-resolution diagnostic methods in ophthalmology that cannot be appreciated with single-photon imaging. It provides a novel opportunity to functionally image pathological changes in lipofuscin granules concentration and monitor cellular biochemical activity at a subcellular level, which may help in the understanding of the early mechanisms of AMD.

Today, TPEF imaging is particularly widely used in neurology and embryology²⁵⁻²⁷ for vital imaging, but applications in ophthalmology are still in early development.²⁸⁻³⁰ Typical TPEF systems require 1 s or more for a full-frame scan, but many biological processes in cells and tissues undergo much faster changes.³¹ Especially in any clinical ophthalmological applications, where the presence of motion artifacts like eye movements is a concern, high-speed scanning systems are necessary. To the best of our knowledge, there has been no work reported on the application and potential of TPEF imaging through a fast-scanning ophthalmoscope toward real-time *in vivo* applications in the eye.

We previously reported on two-photon excited autofluorescence imaging on *ex vivo* human RPE cells through a commercial multiphoton laser scanning microscope (Zeiss LSM 510 NLO) to study the morphological and spectral features of the RPE cells.²⁹ The present study focuses on the development of a novel custom-made two-photon laser scanning ophthalmoscope for the study of the feasibility of a high-speed

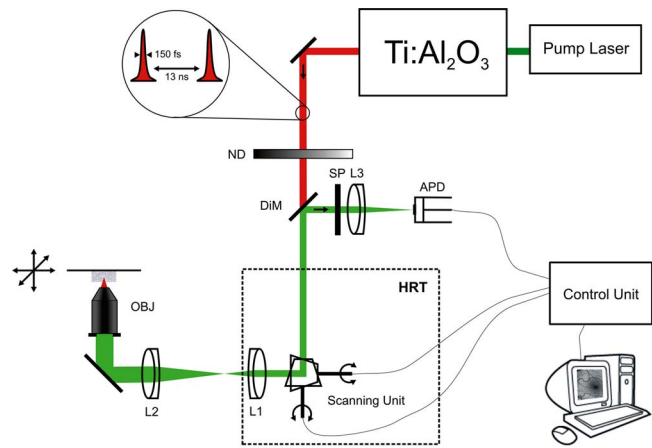


Fig. 1 Optical diagram for high-speed TPEF imaging based on a conventional scanning laser ophthalmoscope. Main components: mode-locked Ti:sapphire fs laser (Coherent Mira 900), neutral-density filter wheel ND, dichroic mirror DiM (Semrock), scanning unit (HRT, Heidelberg Engineering), scan lens L1, tube lens L2, objective lens OBJ ($40\times/0.8$ W, Leica), shortpass filter SP (Semrock), and avalanche photodiode APD. The APD (Perkin Elmer) is synchronized to the scanner through the control unit (HRT, Heidelberg Engineering) to construct a digital image from fluorescence intensity measurements at each pixel.

resonant scanning system (20 fps) for a potential *in vivo* application of two-photon FAF imaging in clinical applications. Preliminary TPEF images of the autofluorescent lipofuscin granules from human-donor RPE cells are presented and qualitatively compared to those of a slow-scanning commercial multiphoton laser scanning microscope.

2 Materials and Methods

2.1 Optical Setup for Fast TPEF Imaging

A nonlinear microscope, based on the scanning and detection unit of a conventional scanning laser ophthalmoscope [Heidelberg Retina Tomograph (HRT), Heidelberg Engineering, Germany] with a modified epi-illumination light path, was coupled to a mode-locked Ti:sapphire femtosecond (fs) laser (Coherent Mira 900) pumped by a 532 nm DPSS CW laser (Coherent Verdi V5) to allow fast TPEF imaging of human RPE samples (Fig. 1). Due to the relatively low two-photon excitation cross section, high light intensities are mandatory, which is best achieved with pulsed fs lasers with moderate peak power but low average power.²¹ The Ti:sapphire laser employed has a pulse repetition rate of 76 MHz with pulses of 150 fs and a wavelength tunable from 700 to 980 nm. The maximum average power is about 500 mW and can be linearly adjusted by rotating a reflective neutral density filter wheel in the excitation beam to change the laser power transmitted. The scanners employed are from the original HRT and consist of fast resonant galvanometer mirrors (4 kHz *x*-scan), allowing frame rates up to 20.83 Hz. The original scan-angle range of the conventional HRT was also modified for high-resolution optical “zooming” at scan angles of 10×10 , 5×5 , and 1×1 deg. After the scanning mirrors, a 1:3 Keplerian telescope, consisting of the scan and the tube lens, adjusts the beam size at the back-aperture of the

objective (U-V-I Apochromat, $40\times/0.8$ W, Leica) to assure the lens is overfilled for a diffraction-limited focus on the specimen. The specimen is mounted in a manual *xyz*-translation stage for proper positioning and focusing under the excitation beam.

The blue/green fluorescence light is collected by the same objective lens, descanned, and projected by reflection on a dichroic mirror [designed to transmit the laser light and to reflect the fluorescence light (380–720 nm), Semrock] onto an avalanche photodiode (APD, Perkin Elmer). Backscattered laser light is further rejected by an IR-cut filter (750 nm cut-off wavelength, Optical density >6 , Semrock). The excitation is point-by-point of a square raster scanned region of interest. Because no fluorescence is generated outside the focal volume, a confocal pinhole is left out. The time integration of the APD is synchronized to the scanner through a control unit in order to temporally and spatially reconstruct a digital 8-bit gray-scale image of 256×256 pixels as the laser sweeps across the sample.

For the 10×10 , 5×5 , and 1×1 deg scan angle, the field of view is 430×430 , 215×215 , and $43\times 43\ \mu\text{m}^2$, respectively. The pixel dwell time is $0.50\ \mu\text{s}$. A stack of 32 images is recorded in 1.6 s and subsequently averaged to increase the signal-to-noise ratio. The setup also allows for the exchange of the APD with a spectrometer (USB4000-VIS-NIR, Ocean Optics) with a spectral bandwidth from 350 to 1000 nm to measure the fluorescence emission spectrum of the sample region in focus.

2.2 Sample Preparation

Human retinas were obtained from postmortem donor eyes with normal vision (no fundus pathology) from the Institute of Ophthalmology, University of Bonn, Germany. The posterior half of the eyeball was cut and fixed with paraformaldehyde [4% in phosphate-buffered saline (PBS), pH 7.4]. A 5-mm-diam retina/sclera probe from the macular region was prepared with a surgical trephine. The neural retina was separated from the RPE-choroid-sclera complex. The relative tissue probe was immersed in a custom-made sample holder filled with PBS (pH 7.4) solution and imaged with the large-working-distance water-immersion objective.

3 Results and Discussion

Figure 2 shows a representative series of 57-year-old human-donor RPE cells imaged by TPEF. Images in Figs. 2(a)–2(c) were recorded through the fast-scanning nonlinear ophthalmoscope-based microscope described above for different scan angles (10×10 , 5×5 , and 1×1 deg, respectively). Each consists of an averaged stack of 32 consecutive images; no further image processing has been done. The excitation wavelength of the Ti:sapphire laser was set to 830 nm, and the average power at the sample was ~ 4 mW. Single lipofuscin granules can clearly be revealed in two-photon autofluorescence with our system. Their typical diameter is $\sim 1\ \mu\text{m}$ and cell size is ~ 15 – $20\ \mu\text{m}$. They accumulate in the cell cytoplasm, being most prominent along the cell membrane. The emission spectrum of the RPE cells in focus excited by 830 nm is given in Fig. 3. The emission ranges from 445 to ~ 760 nm and peaks around 575 nm. This is in good agreement with previously published results on single-photon

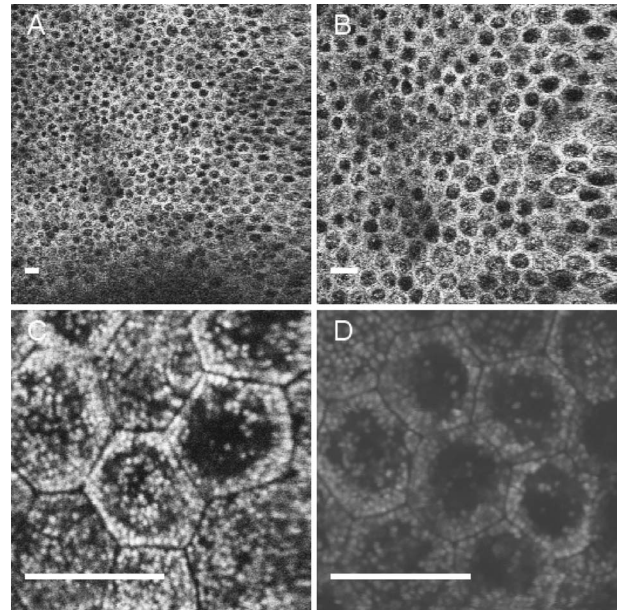


Fig. 2 Two-photon excited autofluorescence imaging of RPE cells of a 57-year-old human-donor eye in the macula region, through the high-speed two-photon ophthalmoscope for (a) 10×10 , (b) 5×5 , and (c) 1×1 deg and (d) through a slow-scanning commercial two-photon microscope (Zeiss LSM 510 NLO). Excitation wavelength 830 nm. Scale bar $20\ \mu\text{m}$.

excited fluorescence emission spectra from lipofuscin^{16,32} and, furthermore, gives a clear indication that the images recorded do originate from a two-photon excitation process.

Figure 2(d) shows a similar cell region within the same sample imaged by two-photon excited autofluorescence through a slow-scanning commercial multiphoton laser scanning microscope (Zeiss LSM 510 NLO) equipped with a Ti:sapphire fs laser (Coherent Cameleon XR), operating at 80-MHz pulse repetition rate, at comparable excitation power (~ 4 mW at the sample) and wavelength (830 nm). One single 256×256 pixel frame was acquired through a $40\times/0.8$ W objective (Zeiss) at a dwell time of $409.46\ \mu\text{s}/\text{pixel}$, compared to $0.50\ \mu\text{s}/\text{pixel}/\text{frame}$ for our high-speed scanning system. The autofluorescence signal was

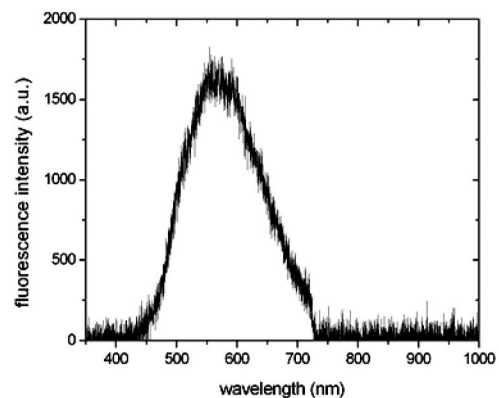


Fig. 3 Two-photon excited autofluorescence emission spectrum of human RPE cells excited by a Ti:sapphire fs laser at 830 nm.

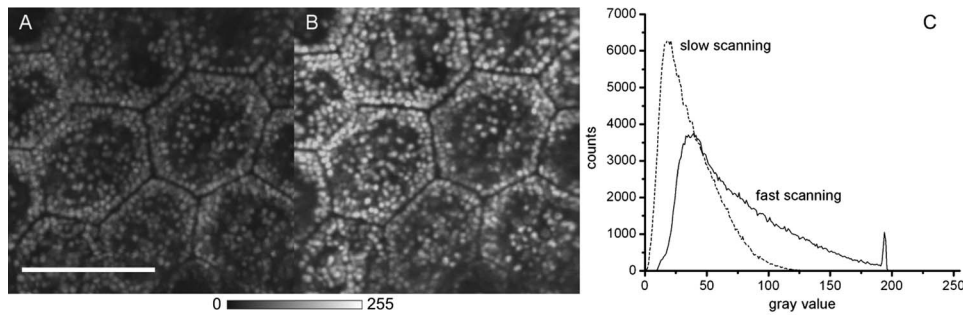


Fig. 4 Two-photon excited autofluorescence imaging of human RPE cells through a commercial two-photon microscope (Zeiss LSM 510 NLO) for different dwell times of 204.73 $\mu\text{s}/\text{pixel}$ (a) and 0.80 $\mu\text{s}/\text{pixel}/\text{frame}$ (256 averaged frames) (b). Scale bar 20 μm . Histogram of counts per gray value of the images in A and B (c).

detected by two photodetectors assigned to different spectral windows, namely, 500–550 and 575–640 nm. The images from the fast-scanning ophthalmoscope look comparable to, if not brighter, than, those recorded with the slow-scanning system. Although not quantitatively comparable, because they are dependent on the settings of the relative detection unit, our results prove that despite the short pixel dwell time of our system, enough fluorescent photons at moderate excitation power can be generated to produce a meaningful record of the lipofuscin concentration and spatial distribution within the RPE cells, with the advantage of video-frame rate imaging.

To further analyze the dependency of fluorescence yield and image brightness on scan speed, we took two consequent images at different scan speeds on the Zeiss microscope at equal excitation power and detector settings from the same specimen (Fig. 4). One 512×512 pixels frame of $43 \times 43 \mu\text{m}$ was recorded with a dwell time of 204.73 $\mu\text{s}/\text{pixel}$ [Fig. 4(a)]. A second image with a dwell time of 0.80 $\mu\text{s}/\text{pixel}/\text{frame}$ was averaged over 256 frames [Fig. 4(b)] so that the total dwell time was 204.80 $\mu\text{s}/\text{pixel}$ for 256 frames, and thus, the same amount of pulses reached a molecule in both cases but at different time intervals. In both images, the corresponding dark image was subtracted. The brightness histogram [Fig. 4(c)] shows an approximately two-fold brighter image in the fast-scanning mode compared to the slow-scanning mode. This can be explained by taking a closer look at the photophysics of the fluorescent molecules involved in the excitation process.

For the 0.8 numerical aperture objective, the diffraction-limited $1/e$ -width w of the squared illumination point spread function is 0.467 μm [calculated from $w = \sqrt{2}(0.325\lambda/NA^{0.91})$, see Ref. 22]. This is the effective illumination space where two-photon excitation takes place. As the laser sweeps across the sample, a molecule is illuminated during the time $t_{\text{eff}} = w/v$, where v is the velocity in the focal plane. Applying a four-state fluorescence model³³ (Fig. 5), a fluorophore faced to an excitation laser pulse is excited by the simultaneous absorption of two photons from its ground state S_0 to the excited state S_1 . Fluorescence then occurs upon relaxation from S_1 back to the ground state, or the fluorophore gets trapped in a relatively long-lived triplet state T_1 , which can relax, with or without emission of a photon, back to S_0 or undergoes photodissociation and irreversibly exits the fluorescence process to a bleached state. Further excitations of T_1 to

an excited triplet state $T_{n>1}$, as well as the absorption of a second photon pair in the excited singlet state, are assumed to all degrade into a bleached state. The typical fluorescence lifetime of organic fluorophores is in the order of 1–10 ns, whereas excited triplet-state lifetimes are typically in the order of 10^{-3} – 10^{-6} s.³⁴ In the slow-scanning mode, with a pixel dwell time of 204.73 μs , each fluorescent molecule is confronted to ~ 90000 consecutive pulses, compared to ~ 400 pulses for the fast-scanning mode with a pixel dwell time of 0.80 μs . Once this molecule is in T_1 , it cannot relax to the ground state S_0 before the next pulse hits it and is likely to be bleached. A schematic illustration of the fluorescence yield over the pixel dwell time for the fast- and the slow-scanning mode is given in Fig. 6. The longer the effective illumination time of the fluorophores t_{eff} , compared to the excited triplet-state lifetime, the more fluorophores are quenched in dark states that do not contribute to the fluorescence process and consequently lower the effective fluorescence signal per pixel.

Donnert et al.³⁵ demonstrated that reducing the pulse repetition rate of the excitation laser below 1 MHz (i.e., pulse intermission $> 1 \mu\text{s}$) allowed transient molecular dark states of similar lifetimes to relax between two molecular absorption events and consequently increased the total number of photons emitted by a dye. These findings suggest that fast-scanning devices may produce similar results. The ideal scan speed would require succeeding pulses to illuminate different molecules. This is achieved for an effective illumination time shorter than $t_{\text{eff}} = 12.5$ ns. Our results, however, indicate that a relief can already be expected for lower speeds, because they

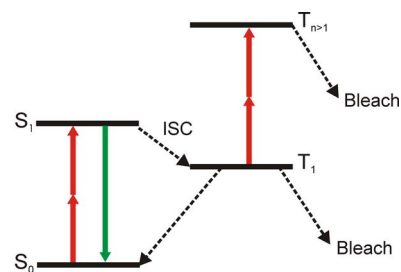


Fig. 5 Four-state energy diagram indicating the major molecular pathways of a fluorescent molecule upon absorption of a photon pair: singlet states S_0 and S_1 , triplet states T_1 and $T_{n>1}$, intersystem crossing (ISC), and photobleaching (bleach).

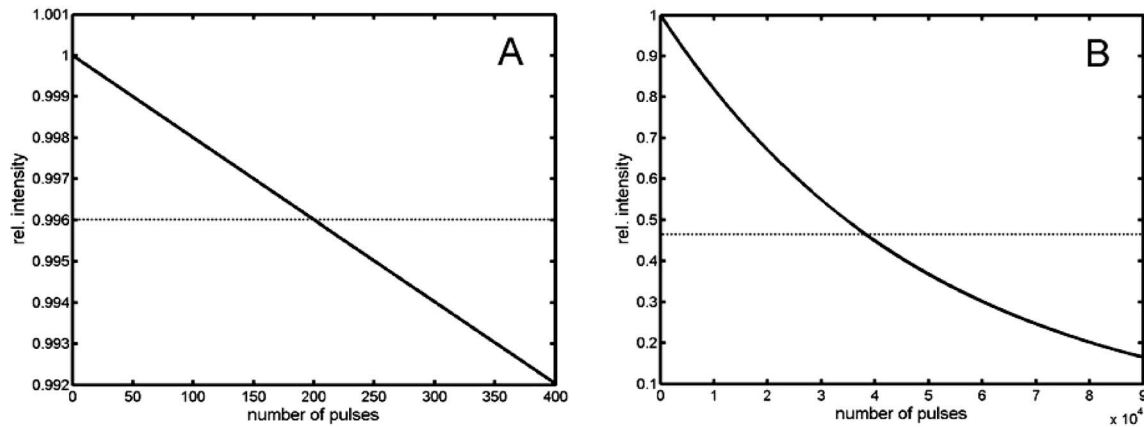


Fig. 6 Schematic illustration of the fluorescence yield dependency on pixel dwell time for the fast-scanning mode, i.e., 400 pulses per pixel (a), and the slow-scanning mode, i.e., 90000 pulses per pixel (b). The dotted line represents the averaged fluorescence over the respective pixel dwell time.

already reduce effective triplet buildup. Consequently, the gain in excitation efficiency might explain the strong fluorescence signal achieved with the resonant ophthalmoscopic scanner ($t_{\text{eff}}=1.39 \mu\text{s}$, i.e., 106 pulses per molecule at 1 deg scan angle) described above.

4 Conclusion

The results of this study demonstrate that TPEF imaging of human-donor RPE cells can be achieved by a fast-scanning ophthalmoscope and are a first step from two-photon microscopy toward two-photon ophthalmoscopy. Lipofuscin granules show strong two-photon autofluorescence when excited with a Ti:sapphire laser at 830 nm. Besides better depth penetration and the transparency of the human eye to NIR light, TPEF offers a number of advantages for vital imaging that cannot be appreciated with single-photon excited fluorescence.

Living-eye imaging for clinical applications, however, necessitates further considerations on laser exposure. The relative effectiveness of NIR light to cause retinal damage is much less as compared to blue excitation light, but the existence of single-photon absorbing melanin granules (in the RPE and choroid) in the NIR wavelength band can potentially cause photothermal damage.

The ANSI standard³⁶ specifies a maximum permissible exposure (MPE) of $2.8 \times 10^{-8} \text{ J/cm}^2$ (i.e., 70.5 kW peak power), corresponding to an average illumination power of 0.8 W at the cornea, for a single 150 fs pulse at 830 nm. At high pulse-repetition rates ($>55.5 \text{ kHz}$), the damage threshold is anticipated to approach the continuous-wave (CW) laser threshold with the same average power. A common simulation for the MPE of a scanning laser ophthalmoscope is that of a CW beam uniformly dispersed over the entire retinal scanning field.³⁷ With the above parameters, an intrapupillary radiant power of 9 mW is permissible for an illumination time of 1.6 s (i.e., 32 images). This limitation should be considered for the design of the nonlinear SLO for living-eye applications. As the two-photon excitation laser only needs to be switched on during image acquisition, a low-power laser di-

ode in reflection mode should be implemented to align the retinal exposure site when trying to minimize retinal exposure.

In order to profit from the full numerical aperture of the eye and maximize the efficiency of the two-photon excitation process while minimizing retinal exposure to radiation, a combination of the TPEF imaging system with adaptive optics able to compensate for “large-pupil” aberrations will be mandatory to make TPEF practically feasible for *in vivo* retinal imaging. By considering triplet-state excitations, fast scanning in TPEF is likely to increase fluorescence yield and image brightness as compared to slow-scanning systems. This is beneficial to any nonlinear ophthalmologic application, where interframe eye motion is a concern and a fast-scanning system is required.

In summary, regarding the present *ex vivo* results, we believe that high-speed TPEF on endogenous fluorophores like lipofuscin will pave the way for a new efficient ophthalmologic diagnostic technique with tremendous potential for non-invasive, functional, high-resolution imaging of the ocular fundus, which may provide new insights into the understanding of the early mechanisms that trigger RPE-related diseases such as AMD at a subcellular level.

Acknowledgments

The authors thank Heidelberg Engineering GmbH (Heidelberg, Germany), Professor W. Denk for using his laser system and microscope facility at the Max-Planck Institute for Medical Research, Heidelberg, and Professor F. G. Holz from the Department of Ophthalmology, University of Bonn, Germany for providing the postmortem human-retina samples. This research was supported with a scholarship from the Ministère de la Culture, de l'Enseignement Supérieur et de la Recherche, G.-D. de Luxembourg and the Centre de Recherche Public Gabriel Lippmann.

References

1. O. Strauss, “The retinal pigment epithelium in visual function,” *Physiol. Rev.* **85**(3), 845–881 (2005).
2. M. L. Katz and G. E. Eldred, “Retinal light damage reduces autofluorescent pigment deposition in the retinal pigment epithelium,”

- Invest. Ophthalmol. Visual Sci.* **30**(1), 37–43 (1989).
3. M. Boulton, N. M. McKechnie, J. Breda, M. Bayly, and J. Marshall, "The formation of autofluorescent granules in cultured human RPE," *Invest. Ophthalmol. Visual Sci.* **30**(1), 82–89 (1989).
 4. F. C. Delori, D. G. Goger, and C. K. Dorey, "Age-related accumulation and spatial distribution of lipofuscin in RPE of normal subjects," *Invest. Ophthalmol. Visual Sci.* **42**(8), 1855–1866 (2001).
 5. R. W. Young, "Pathophysiology of age-related macular degeneration," *Surv. Ophthalmol.* **31**(5), 291–306 (1987).
 6. J. R. Sparrow, K. Nakanishi, and C. A. Parish, "The lipofuscin fluorophore A2E mediates blue light-induced damage to retinal epithelial cells," *Invest. Ophthalmol. Visual Sci.* **41**(7), 1691–1699 (2000).
 7. C. K. Dorey, G. Wu, D. Ebenstein, A. Garsd, and J. J. Weiter, "Cell loss in the aging retina. Relationship to lipofuscin accumulation and macular degeneration," *Invest. Ophthalmol. Visual Sci.* **30**(8), 1691–1699 (1989).
 8. F. G. Holz, F. Schütt, J. Kopitz, G. E. Eldred, F. E. Kruse, H. E. Volcker, and M. Cantz, "Inhibition of lysosomal degradative functions in RPE cells by a retinoid component of lipofuscin," *Invest. Ophthalmol. Visual Sci.* **40**(3), 737–743 (1999).
 9. F. Schütt, S. Davies, J. Kopitz, F. G. Holz, and M. E. Boulton, "Photodamage to human RPE cells by A2-E, a retinoid component of lipofuscin," *Invest. Ophthalmol. Visual Sci.* **41**(8), 2303–2308 (2000).
 10. R. Klein, B. E. Klein, and K. L. Linton, "Prevalence of age-related maculopathy: The beaver dam eye study," *Ophthalmology* **99**(6), 933–943 (1992).
 11. A. von Rückmann, F. W. Fitzke, and A. C. Bird, "In vivo fundus autofluorescence in macular dystrophies," *Arch. Ophthalmol. (Chicago)* **115**(5), 609–615 (1997).
 12. Frank G. Holz, "Autofluorescence imaging of the macula," *Ophthalmologie* **98**(1), 10–18 (2001).
 13. F. G. Holz, C. Bellman, S. Staudt, F. Schütt, and H. E. Völcker, "Fundus autofluorescence and development of geographic atrophy in age-related macular degeneration," *Invest. Ophthalmol. Visual Sci.* **42**(5), 1051–1056 (2001).
 14. O. Arend, J. J. Weiter, D. G. Goger, and F. C. Delori, "In vivo fundus fluorescence measurements in patients with age-related macular degeneration," *Ophthalmologie* **92**(5), 647–653 (1995).
 15. A. von Rückmann, F. W. Fitzke, and A. C. Bird, "Fundus autofluorescence in age-related macular disease imaged with a laser scanning ophthalmoscope," *Invest. Ophthalmol. Visual Sci.* **38**(2), 478–486 (1997).
 16. F. C. Delori, C. K. Dorey, G. Staurengi, O. Arend, D. G. Goger, and J. J. Weiter, "In vivo fluorescence of the ocular fundus exhibits retinal pigment epithelium lipofuscin characteristics," *Invest. Ophthalmol. Visual Sci.* **36**(3), 718–729 (1995).
 17. F. C. Delori, D. G. Goger, and K. C. Dorey, "Age-related accumulation and spatial distribution of lipofuscin in RPE of normal subjects," *Invest. Ophthalmol. Visual Sci.* **42**(8), 1855–1866 (2001).
 18. F. C. Delori, M. R. Fleckner, D. G. Goger, J. J. Weiter, and C. K. Dorey, "Autofluorescence distribution associated with drusen in age-related macular degeneration," *Invest. Ophthalmol. Visual Sci.* **41**(2), 496–504 (2000).
 19. M. Göppert-Mayer, "Über Elementarakte mit zwei Quantensprüngen," *Ann. Phys.* **401**(3), 273–294 (1931).
 20. W. Kaiser and C. G. B. Garrett, "Two-photon excitation in $\text{CaF}_2:\text{Eu}^{2+}$," *Phys. Rev. Lett.* **7**(6), 229–231 (1961).
 21. W. Denk, J. H. Strickler, and W. W. Webb, "Two-photon laser scanning fluorescence microscopy," *Science* **248**(4951), 73–76 (1990).
 22. W. R. Zipfel, R. M. Williams, and W. W. Webb, "Nonlinear magic: multiphoton microscopy in the biosciences," *Nat. Biotechnol.* **21**(11), 1369–1377 (2003).
 23. V. E. Centonze and J. G. White, "Multiphoton excitation provides optical sections from deeper within scattering specimens than confocal imaging," *Biophys. J.* **75**(4), 2015–2024 (1998).
 24. A. Periasamy, P. Skoglund, C. Noakes, and R. Keller, "An evaluation of two-photon excitation versus confocal and digital deconvolution fluorescence microscopy imaging in xenopus morphogenesis," *Microw. Res. Tech.* **47**(3), 172–181 (1999).
 25. W. Denk, K. R. Delaney, A. Gelperin, D. Kleinfeld, B. W. Strowbridge, D. W. Tank, and R. Yuste, "Anatomical and functional imaging of neurons using 2-photon laser scanning microscopy," *J. Neurosci. Methods* **54**(2), 141–162 (1994).
 26. Z. F. Mainen, M. Maletic-Savatic, S. H. Shi, Y. Hayashi, R. Malinow, and K. Svoboda, "Two-photon imaging in living brain slices," *Methods* **18**(2), 231–239 (1999).
 27. J. M. Squirrell, D. L. Wokosin, J. G. White, and B. D. Bavister, "Long-term two-photon fluorescence imaging of mammalian embryos without compromising viability," *Nat. Biotechnol.* **17**(8), 763–767 (1999).
 28. Y. Imanishi, M. L. Batten, D. W. Piston, W. Baehr, and K. Palczewski, "Noninvasive two-photon imaging reveals retinyl ester storage structures in the eye," *J. Cell Biol.* **164**(3), 373–383 (2004).
 29. M. Han, A. Bindewald-Wittich, F. G. Holz, G. Giese, M. H. Niemz, S. Snyder, H. Sun, J. Yu, M. Agopov, O. La Schiazza, and J. F. Bille, "Two-photon excited autofluorescence imaging of human retinal pigment epithelial cells," *J. Biomed. Opt.* **11**(1), 010501 (2006).
 30. M. Han, G. Giese, S. Schmitz-Valckenberg, A. Bindewald-Wittich, F. G. Holz, J. Yu, J. F. Bille, and M. H. Niemz, "Age-related structural abnormalities in the human retina-choroid complex revealed by two-photon excited autofluorescence imaging," *J. Biomed. Opt.* **12**(2), 024012 (2007).
 31. G. Y. Fan, H. Fujisaki, A. Miyawaki, R. K. Tsay, R. Y. Tsien, and M. H. Ellisman, "Video-rate scanning two-photon excitation fluorescence microscopy and ratio imaging with cameleons," *Biophys. J.* **6**(5), 2412–2420 (1999).
 32. F. C. Delori, K. A. Fitch, and J.-M. Gorrand, "In vivo characterization of intrinsic fundus fluorescence," in *Noninvasive Assessment of the Visual System*, OSA Technical Digest Series, Vol. 3, pp. 72–74, Optical Society of America, Washington, DC (1990).
 33. R. T. Borlinghaus, "MRT letter: high speed scanning has the potential to increase fluorescence yield and to reduce photobleaching," *Microw. Res. Tech.* **69**(9), 689–692 (2006).
 34. A. Diaspro, G. Chirico, C. Usai, P. Ramoino, and J. Dobrucki, "Photobleaching," *Handbook of Biological Confocal Microscopy*, 3rd ed., J. B. Pawley, Ed., pp. 690–702, Springer Science +Business Media, New York (2006).
 35. G. Donnert, C. Eggeling, and S. W. Hell, "Major signal increase in fluorescence microscopy through dark-state relaxation," *Nat. Methods* **4**(1), 81–86 (2007).
 36. ANSI, "American national standard for safe use of lasers (ANSI Z136.1-2000)," Laser Institute of America (2000).
 37. F. C. Delori, R. H. Webb, and D. H. Sliney, "Maximum permissible exposures for ocular safety (ANSI 2000), with emphasis on ophthalmic devices," *J. Opt. Soc. Am. A* **24**(5), 1250–1265 (2007).